ACS Biomaterials SCIENCE & ENGINEERING

pubs.acs.org/journal/abseba

Article

Tuning the Biodegradation Rate of Silk Materials via Embedded Enzymes

Junqi Wu,[‖] Kareen A. Fajardo Cortes,[‖] Chunmei Li,*[,‖] Yushu Wang, Chengchen Guo, Kaveh Momenzadeh, Diana Yeritsyan, Philip Hanna, Aron Lechtig, Ara Nazarian, Samuel J. Lin,* and David L. Kaplan*

Cite This: *ACS Biomater. Sci. Eng.* 2024, 10, 2607−2615

Read Online

ACCESS | Metrics & More | Article Recommendations | Supporting Information

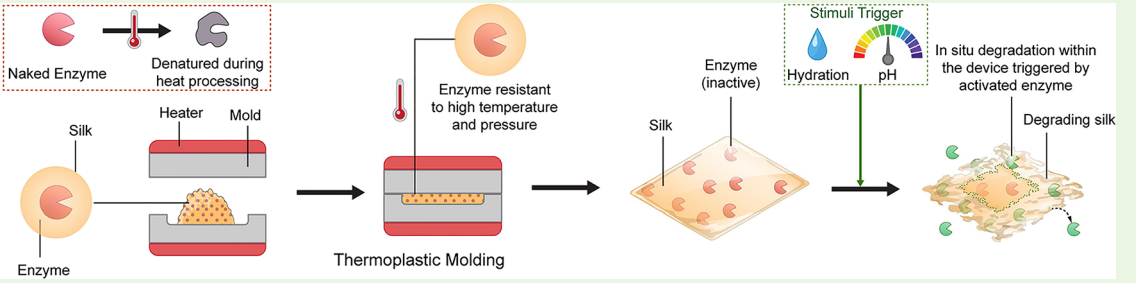

ABSTRACT: Conventional thinking when designing biodegradable materials and devices is to tune the intrinsic properties and morphological features of the material to regulate their degradation rate, modulating traditional factors such as molecular weight and crystallinity. Since regenerated silk protein can be directly thermoplastically molded to generate robust dense silk plastic-like materials, this approach afforded a new tool to control silk degradation by enabling the mixing of a silk-degrading protease into bulk silk material prior to thermoplastic processing. Here we demonstrate the preparation of these silk-based devices with embedded silk-degrading protease to modulate the degradation based on the internal presence of the enzyme to support silk degradation, as opposed to the traditional surface degradation for silk materials. The degradability of these silk devices with and without embedded protease XIV was assessed both in vitro and in vivo. Ultimately, this new process approach provides direct control of the degradation lifetime of the devices, empowered through internal digestion via water-activated proteases entrained and stabilized during the thermoplastic process.

KEYWORDS: *enzyme embedding, degradation, bioplastic, silk*

1. INTRODUCTION

Silk, a natural protein-based biopolymer, presents unique advantages in terms of biodegradability with controlled degradation kinetics and low immunogenic responsive degradation products.[1−5] Silk degrades in vitro and in vivo in response to proteolytic enzymes, which makes it a good biomaterial candidate for the development of customized medical devices. Biopolymers like silk, particularly dense silk materials with limited porosity such as natural silk fibers, regenerated silk films, and blocks, follow protease-mediated surface degradation, where the peptide bond digestion happens in a layer-by-layer fashion from the surface to bulk. This surface erosion is slow, with the rate dependent on the molecular weight, crystallinity, and the specific enzyme.[6] The on-demand degradation of silk biomaterials remains challenging due to the slow erosion of these dense silk materials. In contrast, synthetic degradable materials (e.g., aliphatic polyesters) as biomaterials for medical devices often exhibit uncontrollable degradation kinetics due to bulk hydrolysis and undesirable degradation products, resulting in unwanted inflammatory responses.[7−9]

With recent advances in processing, silk can now be engineered into mechanically robust, dense, plastic-like bulk materials with outstanding machinability, providing a path toward the fabrication of a new class of biodegradable orthopedic devices with good control over degradation rate.[10−15] By tuning the processing parameters, silk thermoplastic molding can generate bulk silk materials with molecular structures and physical properties required to fabricate silk bone screws and plates for implantation.[10] Importantly, labile biomolecules can withstand the high process temperatures

Received: December 18, 2023
Revised: February 26, 2024
Accepted: February 28, 2024
Published: March 13, 2024

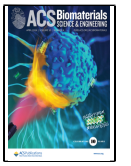

(>100 °C) and pressures (632 MPa) involved in generating these thermoplastic-molded silk materials, maintaining their activity. This stability is due to a combination of the silk chemical structure as a high molecular weight amphiphilic protein, as well as the low water content in the final devices.[10,16,17]

In the present paper, we demonstrate the idea of on-demand degradation of silk materials, which is realized by thermoplastic molding of silk devices with silk-degrading enzymes embedded in the system (Figure 1). Subsequently, the water intrusion or

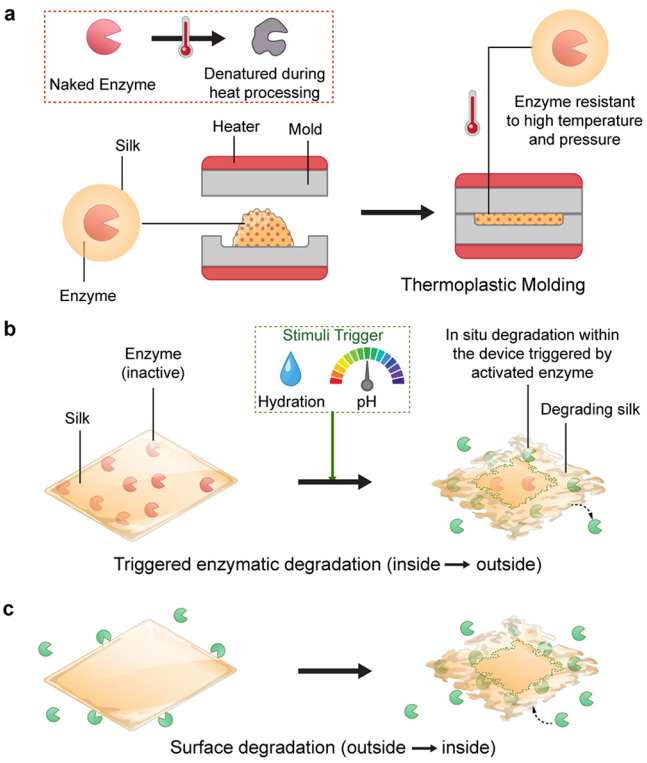

Figure 1. Schematics of enzyme embedding via silk thermal processing and activation triggered silk degradation. (a) Embedded enzyme can withstand the high temperatures and pressures during silk thermoplastic molding while maintaining its activity. (b) Silk degradation begins within the silk device when the embedded enzyme is activated by stimuli such as hydration or pH changes. Activated enzyme may degrade silk in situ (internally, primary mode) or leach out of the device and degrade silk externally. (c) Silk degradation starts at the surface of the device due to the externally supplemented enzyme.

pH can reactivate these embedded enzymes to regulate the degradation of silk devices. Silk devices typically degrade by surface degradation by proteases, from outside to inside the device. By embedding silk-degrading enzymes within the device, degradation mechanisms are reversed, thus fostering an inside-out degradation of the material. Unlike synthetic polymers, where bulk hydrolysis can result in the collapse of the structure, here the degradation of the silk can be controlled by the amount of embedded protease, thus providing tunable rates of degradation and avoidance of buildup of inflammatory metabolites as peptides and amino acids are the product of the reaction. This tunable capability has important clinical implications for the development of silk-based devices that may be programmed to degrade when used in various parts of the body for different bone or soft-tissue to bone stabilization scenarios.

Here we used this materials engineering approach to tune the rate of degradation of silk-based orthopedic devices. Previous research has demonstrated that protease XIV, α-chymotrypsin, proteinase K, papain, collagenase, and other enzymes degrade silk.[5,10,18−25] Among these, protease XIV is the most efficient for degrading silk materials (both the amorphous domains as well as the β sheet crystalline domains), including natural silk fibers, regenerated silk fibers, films, sponges, hydrogels, and bulk materials.[5,10,18−25] Therefore, we used embedded protease XIV within thermoplastic-molded silk bone screws to study the control of silk degradation in vitro and in vivo. In vitro and in vivo studies showed that the silk materials with embedded proteases efficiently degraded when compared to the control silk materials without enzyme, which demonstrated only surface degradation.

2. RESULTS AND DISCUSSION

2.1. Degradation of Silk Bulk Materials In Vitro. The processing temperature during thermoplastic molding is a key factor in controlling the properties of the final materials. Higher processing temperatures often lead to a higher content of β-sheet structure, thus higher crystallinity and higher mechanical strength.[10] The structural difference in the materials obtained at these different processing temperatures also leads to the differences in degradation kinetics due to this difference in semicrystalline content. Bulk silk materials thermoplastic-molded at 125 and 145 °C possessed robust mechanical properties suitable for orthopedic devices, such as silk bone screws.[10] Here, we explored the efficacy of using embedded proteinase XIV to tune the degradation of silk materials processed at 125 °C and 632 MPa in vitro. The 1% enzyme doping level was determined based on the overall degradation efficiency, mechanical performance of the silk devices (Figure S1), and cell toxicity considerations for in vivo experiments.

In vitro degradation of silk screws embedded with protease XIV was performed by incubation in PBS at 37 °C over time. Three methods were used to monitor the degradation process: (1) digital images to reveal morphological changes of the screws; (2) weight loss of the bone screws to understand degradation kinetics; (3) SEM to reveal micro- and nanoscale morphological changes of the surface and cross sections of the screws. Figure 2a reveals the morphological changes of silk screws at different time points of degradation. The silk devices fabricated via thermal processing exhibit a yellow color, which may be due to several chemical reactions that occur at elevated temperatures. For example, the Maillard reaction between amino acids and sugars in glycoproteins and residual sericin could result in the formation of brown or yellow pigments known as melanoidins, which can give silk a yellowish hue. The oxidation of amino acids such as tyrosines can lead to the formation of colored compounds, contributing to yellowing of the silk material. Additionally, chemical changes caused by protein degradation and cross-linking at high temperatures can alter the optical properties of the silk materials, resulting in color changes, such as yellowing. For bone screws processed without protease, no significant morphological changes were observed within the 30-day degradation period (Figure 2a, A1−A4). In contrast, for the enzyme contained screws, the surface threads of the screws lost features over time, and the screw started to disintegrate at day 30 (Figure 2a, A5−A8).

https://doi.org/10.1021/acsbiomaterials.3c01758
ACS Biomater. Sci. Eng. 2024, 10, 2607−2615

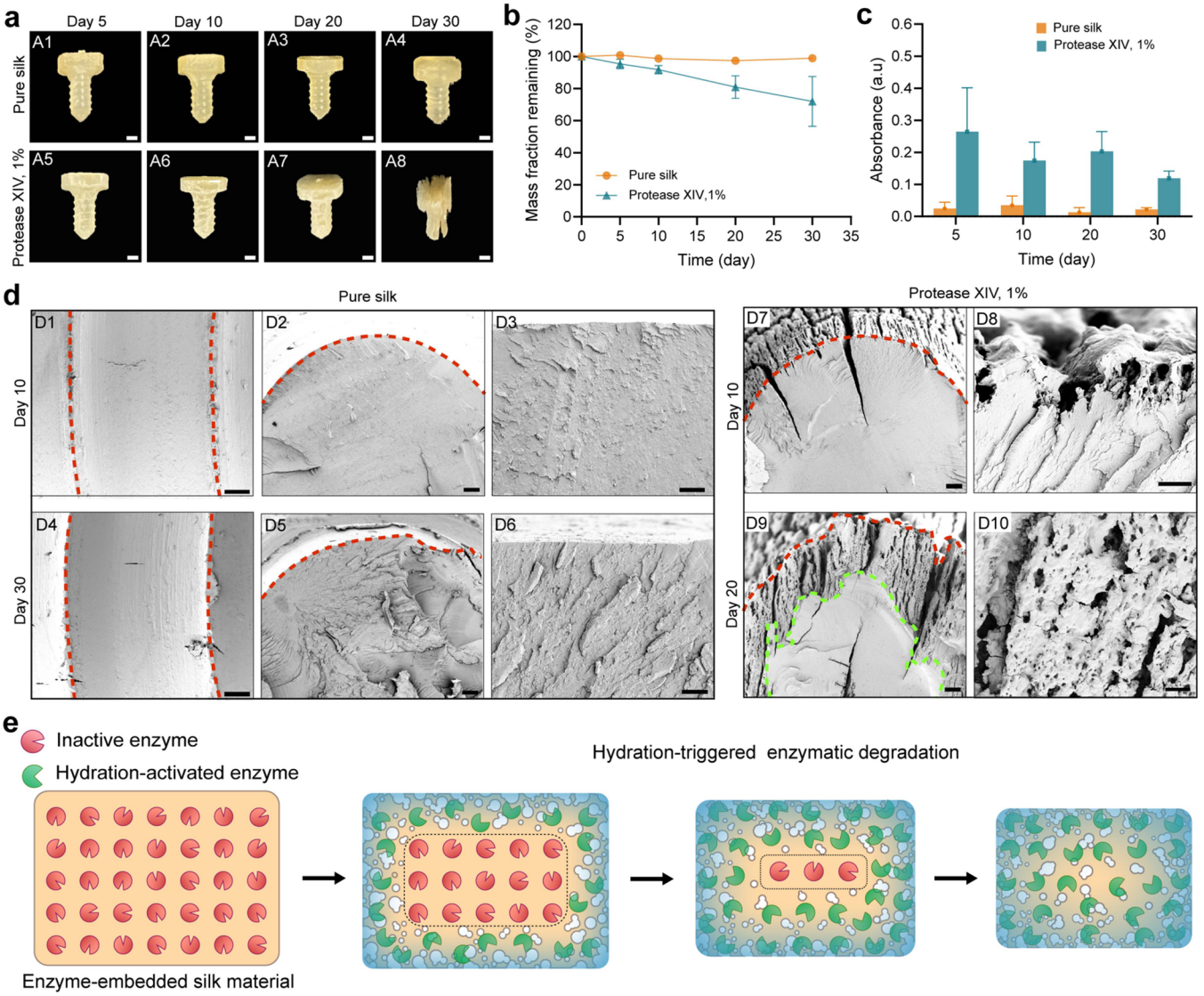

Figure 2. In vitro degradation analysis of silk bone screws with or without embedded protease XIV (1 wt %). The silk bone screws were machined from pure silk and silk−protease XIV materials prepared at 125 °C and 632 MPa. (a) Digital images of pure silk (A1−A4) and silk-protease screws (A5−A8) after incubation in PBS buffer at 37 °C for different durations: A1 and A5, day 5; A2 and A6, day 10; A3 and A7, day 20; A4 and A8, day 30. (b) Remaining mass of silk and silk-protease screws as a function of degradation time in 37 °C PBS buffer (error bars represent standard deviation; $n \geq 3$). Silk degradation in PBS buffer supplemented with protease XIV solution was conducted as a positive control for surface erosion. (c) Protease activity measurement for protease XIV in PBS buffer at various degradation times. (d) SEM images of the surface and cross section of silk (D1−D6) and silk-protease screws (D7−D10) at various degradation times: D1−D3 and D7−D8, day 10; D4−D6, day 30; and D9−D10, day 20. Red dashed lines in D1 and D4 delineate the thread on the screw surface. Red dashed lines in D2, D5, D7, and D9 delineate the periphery of the screw cross section. The green dashed line in part D9 indicates the boundary between the porous zone under degradation and the solid core. (e) Schematic showing hydration-triggered silk degradation over time. The degradation front (black dashed line) advances toward the center of the device with the progression of the hydration zone (blue zone). The scale bars in A1−A8 are 1 mm. The scale bars in D1−D6, D7, and D9 are 100 μm, and the scale bars in D3, D6, D8, and D10 are 10 μm.

Figure 2b shows the weight changes of the screws at various degradation time points. The silk screws without enzyme exhibited negligible weight change after 30 days of incubation in PBS buffer, losing less than 2% of their original weight. This is consistent with previous research on the degradation of dense silk materials such as films and blocks.[12,26] When 1 wt % protease was embedded in the screw, a linear degradation profile was observed with weight loss of approximately 30% after 30 days, indicating the effectiveness of the embedded enzymes in silk degradation.

Knowing that an embedded enzyme can effectively degrade silk, we sought to understand the mechanism of action. We first verified the bioactivity of the protease by monitoring its activity released into the incubation buffer. The embedded protease was initially inactive and was activated when water or buffer diffused into the silk device, and a hydration zone formed. The activated protease started degrading silk in situ within the hydrated zone, while some protease may diffuse out of the hydration zone and be released into the incubation buffer. The released protease would degrade the silk from the surface to the inside. The screws embedded with protease \demonstrated gradual release of the enzyme over the 30-day degradation period (Figure 2c). This finding demonstrates that

https://doi.org/10.1021/acsbiomaterials.3c01758
ACS Biomater. Sci. Eng. 2024, 10, 2607−2615

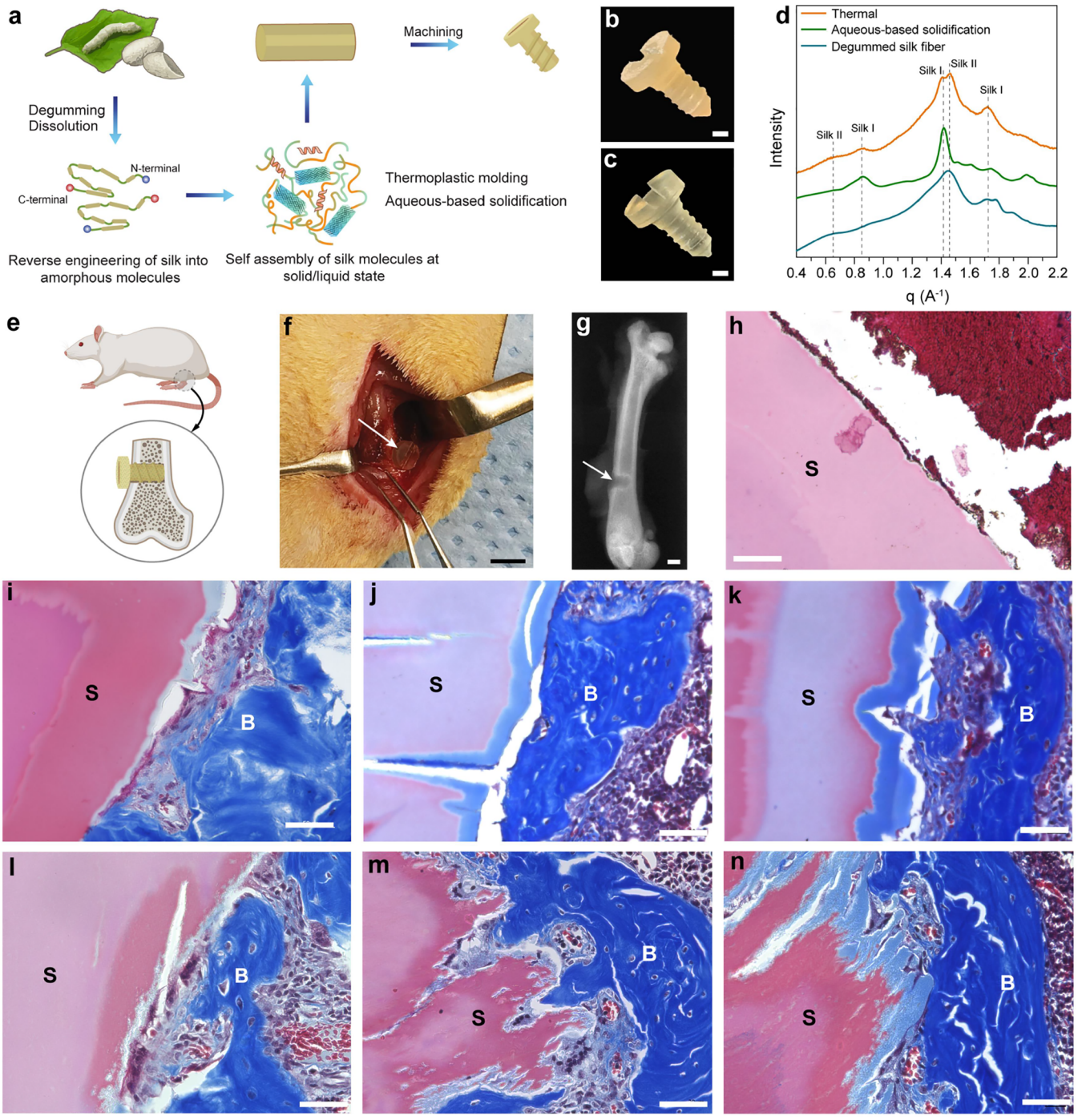

Figure 3. Long-term in vivo degradation of silk screws in a rat femur model (a) Process of generating 3D silk materials and fabrication of silk bone screws. Photographs of silk bone screws prepared by (b) thermoplastic molding and (c) aqueous-based solidification process. (d) One-dimensional WAXS profiles of the bulk silk materials prepared by thermoplastic molding at 145 °C and 632 MPa and aqueous-based solidification process. (e,f) Implantation of silk bone screw and (g) radiograph of rat femur to show the implantation site (white arrow). (h) Masson trichrome stains of cross sections of in vivo silk screws (S) within the medullary cavity (B) at (h) 0, (i,l) 1, (j,m) 6 and (k,n) 12 months after implantation. (h–k) Screws prepared by aqueous-based solidification. (l–n) Screws prepared by thermoplastic molding. Scale bars in parts b and c are 1 mm. Scale bar in f is 5 mm. Scale bar in g is 2 mm. Scale bars in h–n are 50 μm.

the protease's bioactivity was preserved during the silk thermoplastic molding process.

To verify the degradation initiated by the embedded enzyme, SEM was utilized to monitor the morphological changes of the surfaces and cross sections of the silk screws (Figure 2d). At day 0, there were no significant morphological differences between the screws with and without embedded protease (Figure S2). For pure silk screws (no enzyme), consistent with the weight loss results, no discernible degradation was observed within the 30 day degradation period. Both the surface and the cross section of the screws displayed a consistent solid, nonporous structure with sharply defined boundaries. Conversely, by day 5 a thin, porous layer (approximately 12 μm in thickness) emerged on the screws

https://doi.org/10.1021/acsbiomaterials.3c01758
ACS Biomater. Sci. Eng. 2024, 10, 2607–2615

with embedded protease (Figure 2D7,D8). These micro- and nanosized pores were initial indicators of silk degradation. As the degradation continued, the porous zone advanced toward the center of the screw, potentially extending to its core. By day 20, the porous zone exhibited a thickness of approximately 400 μm (Figure 2D9,D10). Thus, water had diffused into the screw, activating the protease and initiating bulk degradation at both micro and nano scales.

A model was proposed to provide insight into the hydration-triggered silk degradation with embedded enzymes based on the experimental observations above. The mechanism is as follows: (1) initially the water content within the thermoplastic molded devices is insufficient for enzyme activation—thus, the protease is inactive postprocessing, (2) upon immersion in water or buffer, water diffuses into the device and activates the embedded protease and a hydration zone forms, (3) the activated enzyme then degrades silk in situ, and (4) silk degradation advances toward the center of the material with the progression of the hydration zone (Figure 2e).

Our previous research has shown that the molding temperature significantly influences the degradation rate of silk-based devices, with increased processing temperatures resulting in slower degradation.[10] For example, silk ear tubes doped with 1 wt % protease XIV manufactured at 145 °C and 632 MPa degrade more slowly than those produced at 125 °C and 632 MPa. This observation may be attributed to two main factors. First, the activity of the temperature-sensitive embedded enzyme may decrease at elevated processing temperatures. Second, the higher crystallinity of silk devices at higher processing temperatures leads to a more compact structure with limited protease accessibility. Additionally, the enzymes can be trapped in the crystalline region during silk self-assembly, making them less accessible to hydration.

Most studies of silk degradation in vitro are conducted by supplementing silk-degrading enzymes externally into the degradation medium, such as in PBS, where the enzyme has to diffuse from the surface into the bulk of the silk materials for degradation, and this process requires frequent replenishment of fresh enzyme in the degradation medium due to loss of enzyme or enzyme activity over time. Here, we demonstrate that embedding enzymes into the bulk silk material induced degradation at the surface as well as in the bulk, without any replenishment required, resulting in accelerated degradation. Notably, the data demonstrate the stabilization of the enzyme within the silk matrix. A similar strategy has been used to modulate the degradation of nonporous, dense films of synthetic polymers such as poly(caprolactone) (PCL) and poly(lactic acid) PLA.[27−31] Accelerated bulk degradation was achieved by embedding *Burkholderia cepacia* lipase (BC-lipase) and *Candida antarctica* lipase (CA-lipase) in PCL, and proteinase K in PLA.[27] We envision that this approach of embedding enzymes within bulk material is a general strategy to control lifetime. This approach can be further extended but utilizes enzymes that activate under specific conditions to provide further control of the lifetime. For example, we demonstrate this control via embedding pepsin, a pH-sensitive protease, in silk rods via thermoplastic molding. As shown in Figure S3, silk degradation was significantly increased when the rods were immersed in acidic PBS (pH = 2) solution in comparison to neutral PBS solution.

2.2. In Vivo Degradation of Pure Silk Bulk Materials in a Rat Femur Model. Next, using a rat femur defect model, we studied the degradation of pure silk bulk materials and evaluated the efficacy of the embedded protease to tune the degradation of silk materials in vivo. We first conducted a 12-month study to investigate the natural degradation of pure silk bulk materials (Figure 3). Silk screws prepared via two different processes: thermoplastic molding at 145 °C and 632 MPa and aqueous-based solidification were used in the study. Wide-angle X-ray scattering (WAXS) analysis showed that the silk materials from thermoplastic molding possessed mainly a silk II structure (as in degummed silk fibers), whereas silk materials from the aqueous-based solidification process possessed mainly a silk I structure (Figure 3d).[10]

Despite the structural differences, the two bulk silk materials had comparable mechanical strength.[10,11] The silk screws were machined from two types of bulk silk materials and implanted in rat femurs. For this phase of the study, no proteases were added to the material. No screws failed during implantation and all screws were inserted in the same manner as current metallic devices, where a pilot hole was predrilled and the screw inserted without pretapping (creation of screw thread pathway) of the hole. During implantation, the screws came into contact with blood and the surrounding soft tissue but maintained their mechanical integrity for implantation. We evaluated the degradation of both types of screws with time in vivo. Histology analysis showed that both types of screws underwent slow surface degradation. Surface erosion and cracks were observed on the silk materials one month after implantation (Figure 3i,l). Enhanced roughness and cracks developed in a surface-to-interior manner from 6 (Figure 3j,m) to 12 months (Figure 3k,n) after implantation. In addition, a porous and less dense region was observed on the surface of the screws, based on the improved uptake of blue staining. These morphological changes can be interpreted as indications of silk degradation in vivo. Multinucleated giant cells were closely associated with the rough and irregular features of the screw surfaces during the degradation process, suggesting the active involvement of the giant cells. Histological analysis showed new bone deposition directly on the screw surfaces without intervening fibrous tissue, suggesting good osteoconductivity by the silk devices. In addition, no significant accumulation of inflammatory cells was detected in the vicinity of the silk screws. The osteoconductive features of the silk screws along with mild inflammation suggest good biocompatibility of silk bone screws.

The degradation of an orthopedic implant needs to be tuned to degrade in a specific window or time frame (6−12 months) in vivo. This ensures adequate mechanical integrity to support bone healing and allows for the dynamic transfer of the mechanical load back to the healing bone during the transition period. The ability to tailor degradation rates is crucial for different areas of the bony skeleton during healing. Given the limited access of phagocytic immune cells to the bulk of screws and plates used in orthopedics, one can expect very slow degradation of silk orthopedic devices in vivo. As demonstrated in this study, despite the difference in processing methods and structure, the in vivo degradation of both types of pure silk screws was slow, with only the surface regions showing signs of degradation over the 12-month period (Figure 3). It is apparent that the dense bulk features of the screws are key to lead to the limited degradation of silk bulk materials in vivo. A similar slow surface degradation was also observed when silk screws prepared using a 1,1,1,3,3,3-Hexafluoro-2-propanol (HFIP) solvent-based process were implanted in rat cranium.[13] Therefore, there was a need to

https://doi.org/10.1021/acsbiomaterials.3c01758
ACS Biomater. Sci. Eng. 2024, 10, 2607−2615

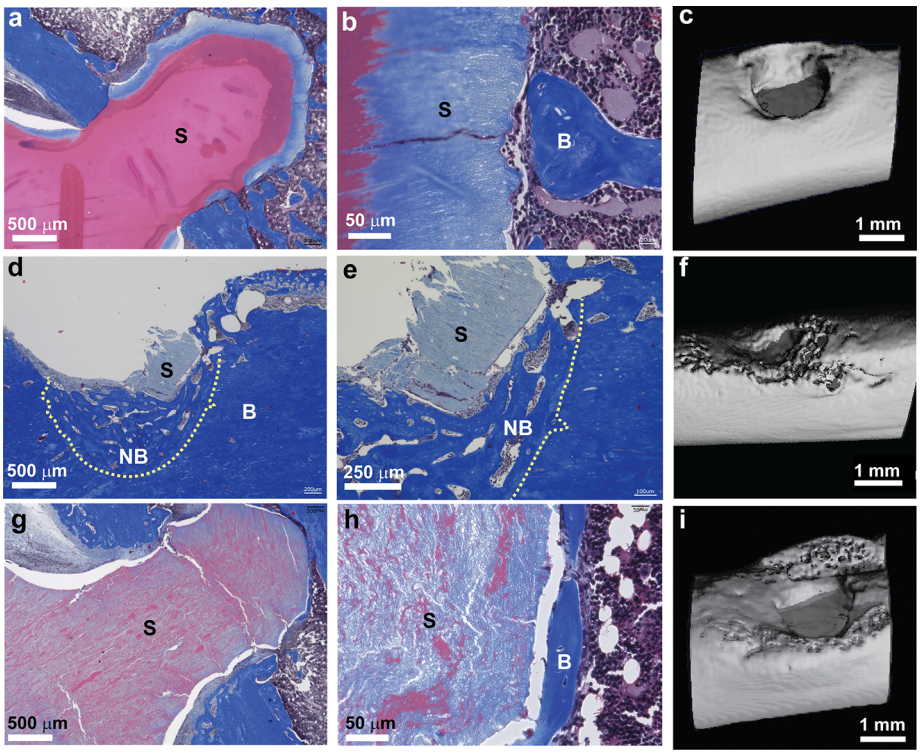

Figure 4. Tuning the in vivo degradation of silk bone screws with embedded protease XIV. Silk screws were machined from thermoplastic molded bulk silk materials. Histology images and microCT of silk screws inserted in rat femurs for 1 month: (a−c) control silk screws without protease XIV, (e−g) silk screws with protease XIV embedded in the bulk material during processing, screw #1, and (i−k) silk screw with bulk-incorporated protease XIV, screw #2. S, silk. B, bone. NB, new bone. The dashed line delineates the boundary between the new and pre-existing bone.

better control the degradation mechanism and lifespan to accelerate the degradation of silk-based orthopedic devices. Proteases represent a growing class of drugs used to harness proteolysis for disease treatment.[32,33] For instance, the proteolytic enzyme collagenase from *Clostridium histolyticum* (CCH) has received FDA approval for treating fibrotic diseases such as palmar fibromatosis.[32,34] We anticipate that incorporating silk-degrading enzymes into dense silk materials, that activate upon hydration or due to a change in pH, can offer a novel tool to tune silk degradation in vivo.

The thermoplastic molding process allows for the incorporation of silk-degrading enzymes with retention of their activity despite the high processing temperatures and pressure.[10] As a proof-of-concept, in the second phase of the in vivo degradation studies, we conducted a one month investigation of the degradation of silk screws (95 °C and 632 MPa) with embedded protease in the rat femur (Figure 4). Silk bulk materials processed at 95 °C have significantly lower β-sheet content and crystallinity than materials processed at 125 and 145 °C;[10] thus, a faster degradation profile was anticipated in vivo. For the control silk screws without sequestered protease (95 °C), degradation occurred by surface erosion, resulting in a porous and less dense zone extending approximately 200 μm into the material from the surface of the screw at one month (Figure 4a,b), whereas the degradation of silk screws processed at 145 °C was confined to a surface zone approximately 5 μm thick (Figure 3i). While screws processed at 95 °C exhibited more advanced degradation than those processed at 145 °C, both types of screws showed a surface degradation pathway; degradation confined to the periphery of the screw, while the bulk was maintained as a solid, nonporous structure. In contrast, the screws with an embedded protease exhibited accelerated degradation. In one representative screw (Figure 4e−g), the shaft of the screw located in the medullary cavity had completely degraded, leaving only a portion of the screw head within the cortical bone. Additionally, the hole in the cortical bone, previously occupied by the degraded screw, was partially filled with new bone tissue (Figure 4e,f). For another screw, typical bulk degradation was evident with the screw displaying a porous and less dense structure throughout (Figure 4i,j). Therefore, in line with our findings from the in vitro study, the embedded protease expedited the degradation of silk bulk materials in vivo by hydration-triggered activation of embedded enzymes. This is especially significant for applications where a controlled and potentially faster rate of degradation is desirable. By embedding protease directly into the silk matrix, we were able to incorporate the material lifetime as a design parameter to better suit specific in vivo applications. Most importantly, this approach overcomes the historical challenges of modulating increased porosity related to increased degradation rate, whereby mechanical properties of the materials then become compromised. Here, the opposite is occurring, where more dense materials stabilize the protease, yet promote increased degradation upon implantation.

Furthermore, direct contact between the newly formed bone and the screw surface was observed in regions where the bone screw was positioned within the medullary cavity. This observation suggests that the introduction of protease into the system did not hinder and was indeed compatible with typical bone healing processes. In contrast to the control screws without protease, evidence of bone remodeling and the presence of fibrous tissue were noted adjacent to portions of the screw within the cortical bone. This could potentially be attributed to excessive interfacial micromotion resulting from

https://doi.org/10.1021/acsbiomaterials.3c01758
ACS Biomater. Sci. Eng. 2024, 10, 2607−2615

the rapid degradation of the screw in juxtaposition with native cortical bone. One limitation of the current study is that silk materials processed at 95 °C were used for in vivo study, which does not represent the full range of the materials' potential in orthopedic applications. Future research will investigate the in vivo degradation pattern of the additional materials processed at 125 and 145 °C to provide insights into their utility.

3. CONCLUSIONS

The continued advancement of degradable orthopedic devices prepared from silk protein faces a contradiction where mechanical strength achieved with denser materials results in slower degradation due to poor diffusion and access of the bulk material. The approach described in the present paper overcomes this challenge, by co-opting the mechanism of degradation from within via sequestered protease that is inactive in the as-prepared materials. This new concept developed in the present work is focused on the development of on-demand tunable degradation, achieved by embedding an inactive enzyme in the system during thermoplastic molding. The embedded enzymes can subsequently be activated by water ingress, or pH, to control the degradation from the inside of the device. We hypothesize that the level of the enzyme loaded into the material can be used to tune the degradation lifetime with a high degree of control. A range of activation triggers can also be designed into the system based on the specificity of the enzyme or exogenous factors. Protease XIV was successfully incorporated into silk-based, dense materials as bone-repair devices through thermoplastic molding. Enzyme activity was maintained despite the high processing temperatures and pressure. The degradation of the bone screws was assessed initially in vitro, where protease embedding enhanced the degradation rate as well as shifted the degradation mechanism from surface only to surface and bulk degradation. Moreover, the efficient bulk degradation of these silk materials with embedded proteases was demonstrated in a rat femur defect model. This enzyme-embedding approach combined with silk thermoplastic molding offers a unique opportunity to modulate silk degradation in vivo to meet the needs of various biomedical applications.

4. EXPERIMENTAL METHODS

4.1. Preparation of Regenerated Silk Solution. Regenerated silk fibroin solution was first extracted from silkworm cocoons according to an established protocol.[35] Briefly, silk cocoons were degummed by boiling in 0.02 M Na_2CO_3 for 30 min, followed by rinsing in distilled water to remove the residue sericin. The degummed silk was then allowed to dry and was subsequently dissolved in 9.3 M LiBr (Sigma-Aldrich) solution at 60 °C for 3−4 h. The solution was then dialyzed (dialysis membranes, MWCO 3500) against distilled water for 2 days with 6 changes of water. After dialysis, the solution was centrifuged at 9780 × *g* for 20 min twice to remove insoluble impurities. The concentration of the final silk solution was about 6 wt %.

4.2. Preparation of Bulk Silk Material via Thermoplastic Molding of Regenerated Silk. Silk solution was diluted with distilled water and frozen in liquid nitrogen, followed by lyophilization at −80 °C and 0.006 bar (Labconco, USA) until complete sublimation. The lyophilized silk was then milled into an ultrafine powder using an analytical mill (20,000 rpm, 2 min, Cole-Parmer). The regenerated silk product obtained was referred to as amorphous silk nanomaterials (ASNs).[10] The ASNs were stored in sealed containers under ambient dry conditions until use. To prepare silk bulk materials, ASNs were packed into predesigned molds and pressed at 632 MPa at the desired temperature (95, 125, or 145 °C) for 15 min. To incorporate protease in the system, ASNs were doped with protease XIV powder (1 wt % of silk, Sigma-Aldrich) by thorough mixing in the analytical mill (20,000 rpm, 1 min, Col-Parmer). The mixture was then subjected to a thermoplastic molding.

4.3. Preparation of Bulk Silk Material via an Aqueous-Based Solidification Process. Silk solution of 6% (w/w) was exposed to forced airflow at 10 °C in a refrigerated incubator to allow water evaporation until silk concentration reached 25−30%.[11] The concentrated silk solution was then loaded into a mold with water-permeable membranes to allow further water evaporation for 3 to 4 days, resulting in solid bulk silk materials. The bulk silk materials were then dried in a fume hood for 4 days followed by 4 days in a 45 °C oven to remove the remaining water.

4.4. Fabrication of Silk Bone Screws. Silk bone screws were machined from bulk silk materials by using a CNC lathe (Trak TRL 1440 EX, Southwestern Industries). A custom single point external cutter (Vargus) was used on the CNC lathe to cut bone screw threads by matching the turning speed with the horizontal speed of the cutter to cut a desired pitch length (outer diameter of ∼1.8 mm and pitch of 600 μm). A cylindrical screw head was machined, and a slot was generated for screw insertion. The dimensions of the screw are illustrated in Figure S4.

4.5. Mechanical Properties. Three-point bending tests were conducted using an Instron 3366 machine (Bruker) at 25 °C and 50% relative humidity (RH) with a loading rate of 0.2 mm min^{-1} min on dry specimens. The specimens had a length of 30 mm, a width of 5 mm, and a thickness of 1.5 mm. Multiple samples (≥3) were tested for each condition.

4.6. In Vitro Degradation Studies and Protease Activity Assay. To monitor the morphological changes of samples during degradation, silk bone screws and screws with embedded protease XIV were incubated in PBS solution (1 mL for each screw) at 37 °C. At designated time points (days 5, 10, 20 and 30), samples were collected, and the dry weights were measured. Digital images were taken at each time point, and the samples were cut to show the cross-section and SEM images collected at each time point. The supernatant was collected at each time point for the protease activity assay (Thermofisher).

4.7. Scanning Electron Microscopy (SEM). The surface and cross-sectional morphologies of the materials were characterized by SEM (Zeiss Gemini 360 FE-SEM). The samples were sputter coated with a thin layer of pt/pd (80:20), and the SEM images were acquired at an acceleration voltage of 5 kV.

4.8. Wide-Angle X-ray Scattering. To investigate the crystalline structure of the silk bulk materials prepared via thermoplastic molding and aqueous-based solidification, WAXS experiments were performed using the BioCars 14BM-C beamline at the Advanced Photon Source at Argonne National Laboratory under proposal GUP-61977. The wavelength of the X-ray beam was 0.979 Å, and the beam size on the sample was 150 × 300 μm (horizontal × vertical). A sample-to-detector distance of 200 mm and a beam stop of 50 mm were used for the measurement. Data were recorded using an ADSC Quantum 315r detector with an exposure time of 10 s. CeO_2 powder was used for instrument calibration.

4.9. In Vivo Degradation Study. The experimental protocols for the animal study were approved by the Institutional Animal Care and Use Committee of Beth Israel Deaconess Medical Center, Boston, MA. Thirteen-week-old female Sprague−Dawley rats (Charles River Laboratories International) were used for the study. After inhalational induction of anesthesia with isoflurane, a 5−10 mm longitudinal incision was made laterally over the distal 1/3 of the femur, followed by incision of the superficial fascia. The intermuscular plane between the vastus lateralis and the biceps femoris muscles was separated to expose the distal end. A unicortical hole was drilled with a Synthes Electric Drive (DePuy Synthes, Inc., West Chester, PA) with a 1.7 mm drill bit. Screws sterilized by ethylene oxide were inserted using a standard flathead screwdriver by self-tapping. Muscles were then approximated using absorbable sutures (Vicryl 5-0) and skin was closed using skin clips. Buprenorphine was administered at a dosage of 1.2 mg kg^{-1} preop and pro re nata (as needed with visible signs of

https://doi.org/10.1021/acsbiomaterials.3c01758
ACS Biomater. Sci. Eng. 2024, 10, 2607−2615

distress). The animals were designated for euthanasia at different time points after surgery in the CO_2 chamber at the animal facility. The operated femur was then retrieved for microcomputed-tomography (CT) and histology analysis.

4.10. Micro-CT Analysis and Histology. The femora were explanted and dissected for MicroCT and histologic analysis. MicroCT scanning was performed using the μCT 40 system (Scanco Medical) as previously described.[10] The distal metaphyseal region of femoral bones was scanned using 55 kV peak potential (kVp), 72 μA current, 250 ms integration time, and 30 μm voxel size. The 3D construction was done by considering 200 slides (6 mm bone segment) centered on the screw shaft.

For histology, the explanted bone specimens were fixed in 10% neutral buffered formalin at room temperature for 48 h. The fixed bone specimens were then decalcified in EDTA for 3−4 weeks until they became flexible. Following decalcification, the tissue was processed with ethanol and xylene and infiltrated with paraffin using an automatic tissue processor. Tissue sections of 5 μm thickness were obtained by sectioning the paraffin blocks along the long axis of the bone and through the screw using a microtome. The tissue sections were then stained with Masson trichrome stain to illustrate the general histology.

■ ASSOCIATED CONTENT

Supporting Information

The Supporting Information is available free of charge at https://pubs.acs.org/doi/10.1021/acsbiomaterials.3c01758.

> Supporting information includes Flexural strength and modulus of the silk plates, their SEM images, pH-controlled on-demand degradation by design, and dimensions of the silk bone screw (PDF).

■ AUTHOR INFORMATION

Corresponding Authors

Chunmei Li − *Department of Biomedical Engineering, Tufts University, Medford, Massachusetts 02155, United States*; Email: chunmei.li@tufts.edu

Samuel J. Lin − *Divisions of Plastic Surgery and Otolaryngology, Beth Israel Deaconess Medical Center, Harvard Medical School, Boston, Massachusetts 02215, United States*; Email: sjlin@bidmc.harvard.edu

David L. Kaplan − *Department of Biomedical Engineering, Tufts University, Medford, Massachusetts 02155, United States*; orcid.org/0000-0002-9245-7774; Email: david.kaplan@tufts.edu

Authors

Junqi Wu − *Department of Biomedical Engineering, Tufts University, Medford, Massachusetts 02155, United States*

Kareen A. Fajardo Cortes − *Department of Biomedical Engineering, Tufts University, Medford, Massachusetts 02155, United States*

Yushu Wang − *Department of Biomedical Engineering, Tufts University, Medford, Massachusetts 02155, United States*

Chengchen Guo − *Department of Biomedical Engineering, Tufts University, Medford, Massachusetts 02155, United States*

Kaveh Momenzadeh − *Center for Advanced Orthopedic Studies, Beth Israel Deaconess Medical Center, Boston, Massachusetts 02215, United States*

Diana Yeritsyan − *Center for Advanced Orthopedic Studies, Beth Israel Deaconess Medical Center, Boston, Massachusetts 02215, United States*

Philip Hanna − *Center for Advanced Orthopedic Studies, Beth Israel Deaconess Medical Center, Boston, Massachusetts 02215, United States*

Aron Lechtig − *Center for Advanced Orthopedic Studies, Beth Israel Deaconess Medical Center, Boston, Massachusetts 02215, United States*

Ara Nazarian − *Center for Advanced Orthopedic Studies, Beth Israel Deaconess Medical Center, Boston, Massachusetts 02215, United States*

Complete contact information is available at: https://pubs.acs.org/10.1021/acsbiomaterials.3c01758

Author Contributions

‖J.W., K.A.F.C., and C.L. contributed equally to this work.

Notes

The authors declare no competing financial interest.

■ ACKNOWLEDGMENTS

This work was supported by grants from the National Institutes of Health (R01AR068048; P41EB027062), the Air Force Office of Scientific Research (FA9550-17-1-0333), and Tufts LaunchpadlAccelerator (TLA) grants.

■ REFERENCES

(1) Li, C.; Wu, J.; Shi, H.; Xia, Z.; Sahoo, J. K.; Yeo, J.; Kaplan, D. L. Fiber-Based Biopolymer Processing as a Route toward Sustainability. *Adv. Mater.* **2022**, *34* (1), No. 2105196.

(2) Li, C.; Guo, C.; Fitzpatrick, V.; Ibrahim, A.; Zwierstra, M. J.; Hanna, P.; Lechtig, A.; Nazarian, A.; Lin, S. J.; Kaplan, D. L. Design of biodegradable, implantable devices towards clinical translation. *Nature Reviews Materials* **2020**, *5* (1), 61−81.

(3) Wu, J.; Sahoo, J. K.; Li, Y.; Xu, Q.; Kaplan, D. L. Challenges in delivering therapeutic peptides and proteins: A silk-based solution. *J. Controlled Release* **2022**, *345*, 176−189.

(4) Wu, J.; Shaidani, S.; Theodossiou, S. K.; Hartzell, E. J.; Kaplan, D. L. Localized, on-demand, sustained drug delivery from biopolymer-based materials. *Expert Opin Drug Deliv* **2022**, *19* (10), 1317−1335.

(5) Horan, R. L.; Antle, K.; Collette, A. L.; Wang, Y.; Huang, J.; Moreau, J. E.; Volloch, V.; Kaplan, D. L.; Altman, G. H. In vitro degradation of silk fibroin. *Biomaterials* **2005**, *26* (17), 3385−3393.

(6) Guo, C.; Li, C.; Kaplan, D. L. Enzymatic Degradation of Bombyx mori Silk Materials: A Review. *Biomacromolecules* **2020**, *21* (5), 1678−1686.

(7) Brannigan, R. P.; Dove, A. P. Synthesis, properties and biomedical applications of hydrolytically degradable materials based on aliphatic polyesters and polycarbonates. *Biomaterials Science* **2017**, *5* (1), 9−21.

(8) Woodard, L. N.; Grunlan, M. A. Hydrolytic Degradation and Erosion of Polyester Biomaterials. *ACS Macro Lett.* **2018**, *7* (8), 976−982.

(9) Rosenboom, J.-G.; Langer, R.; Traverso, G. Bioplastics for a circular economy. *Nature Reviews Materials* **2022**, *7* (2), 117−137.

(10) Guo, C.; Li, C.; Vu, H. V.; Hanna, P.; Lechtig, A.; Qiu, Y.; Mu, X.; Ling, S.; Nazarian, A.; Lin, S. J.; Kaplan, D. L. Thermoplastic moulding of regenerated silk. *Nat. Mater.* **2020**, *19* (1), 102−108.

(11) Li, C.; Hotz, B.; Ling, S.; Guo, J.; Haas, D. S.; Marelli, B.; Omenetto, F.; Lin, S. J.; Kaplan, D. L. Regenerated silk materials for functionalized silk orthopedic devices by mimicking natural processing. *Biomaterials* **2016**, *110*, 24−33.

(12) Perrone, G. S.; Leisk, G. G.; Lo, T. J.; Moreau, J. E.; Haas, D. S.; Papenburg, B. J.; Golden, E. B.; Partlow, B. P.; Fox, S. E.; Ibrahim, A. M. S.; Lin, S. J.; Kaplan, D. L. The use of silk-based devices for fracture fixation. *Nat. Commun.* **2014**, *5* (1), 3385.

(13) Liu, K.; Shi, Z.; Zhang, S.; Zhou, Z.; Sun, L.; Xu, T.; Zhang, Y.; Zhang, G.; Li, X.; Chen, L.; Mao, Y.; Tao, T. H. A Silk Cranial

Fixation System for Neurosurgery. *Adv. Healthcare Mater.* **2018**, *7* (6), No. 1701359.
(14) Zhang, Q.-C.; Ding, W.; Ding, S.-L.; Meng, Q.-B.; Su, D.-H.; Zhang, T.-W.; Chen, Q.; Lian, R.-X.; Zhao, M.-D.; Yu, B.-Q.; Li, X.-L.; Li, Y.-L.; Jiang, L.-B. Robust bioactive protein-based screws with dual crosslinked network for internal bone fixation. *Composites Part B: Engineering* **2022**, *238*, No. 109884.
(15) Yan, Z.; Chen, W.; Jin, W.; Sun, Y.; Cai, J.; Gu, K.; Mi, R.; Chen, N.; Chen, S.; Shao, Z. An interference screw made using a silk fibroin-based bulk material with high content of hydroxyapatite for anterior cruciate ligament reconstruction in a rabbit model. *J. Mater. Chem. B* **2021**, *9* (26), 5352−5364.
(16) Omenetto, F. G.; Kaplan, D. L. New opportunities for an ancient material. *Science* **2010**, *329* (5991), 528−31.
(17) Li, A. B.; Kluge, J. A.; Guziewicz, N. A.; Omenetto, F. G.; Kaplan, D. L. Silk-based stabilization of biomacromolecules. *J. Controlled Release* **2015**, *219*, 416−430.
(18) Arai, T.; Freddi, G.; Innocenti, R.; Tsukada, M. Biodegradation of Bombyx mori silk fibroin fibers and films. *J. Appl. Polym. Sci.* **2004**, *91* (4), 2383−2390.
(19) Brown, J.; Lu, C.-L.; Coburn, J.; Kaplan, D. L. Impact of silk biomaterial structure on proteolysis. *Acta Biomaterialia* **2015**, *11*, 212−221.
(20) Cao, Y.; Wang, B. Biodegradation of Silk Biomaterials. *International Journal of Molecular Sciences* **2009**, *10* (4), 1514−1524.
(21) Holland, C.; Numata, K.; Rnjak-Kovacina, J.; Seib, F. P. The Biomedical Use of Silk: Past, Present, Future. *Adv. Healthcare Mater.* **2019**, *8* (1), No. 1800465.
(22) Li, M.; Ogiso, M.; Minoura, N. Enzymatic degradation behavior of porous silk fibroin sheets. *Biomaterials* **2003**, *24* (2), 357−365.
(23) Lu, Q.; Zhang, B.; Li, M.; Zuo, B.; Kaplan, D. L.; Huang, Y.; Zhu, H. Degradation Mechanism and Control of Silk Fibroin. *Biomacromolecules* **2011**, *12* (4), 1080−1086.
(24) Numata, K.; Cebe, P.; Kaplan, D. L. Mechanism of enzymatic degradation of beta-sheet crystals. *Biomaterials* **2010**, *31* (10), 2926−2933.
(25) Wongpinyochit, T.; Johnston, B. F.; Seib, F. P. Degradation Behavior of Silk Nanoparticles—Enzyme Responsiveness. *ACS Biomaterials Science & Engineering* **2018**, *4* (3), 942−951.
(26) Horan, R. L.; Antle, K.; Collette, A. L.; Wang, Y.; Huang, J.; Moreau, J. E.; Volloch, V.; Kaplan, D. L.; Altman, G. H. In vitro degradation of silk fibroin. *Biomaterials* **2005**, *26* (17), 3385−93.
(27) DelRe, C.; Jiang, Y.; Kang, P.; Kwon, J.; Hall, A.; Jayapurna, I.; Ruan, Z.; Ma, L.; Zolkin, K.; Li, T.; Scown, C. D.; Ritchie, R. O.; Russell, T. P.; Xu, T. Near-complete depolymerization of polyesters with nano-dispersed enzymes. *Nature* **2021**, *592* (7855), 558−563.
(28) Ganesh, M.; Dave, R. N.; L'Amoreaux, W.; Gross, R. A. Embedded Enzymatic Biomaterial Degradation. *Macromolecules* **2009**, *42* (18), 6836−6839.
(29) Greene, A. F.; Vaidya, A.; Collet, C.; Wade, K. R.; Patel, M.; Gaugler, M.; West, M.; Petcu, M.; Parker, K. 3D-Printed Enzyme-Embedded Plastics. *Biomacromolecules* **2021**, *22* (5), 1999−2009.
(30) Huang, Q.; Hiyama, M.; Kabe, T.; Kimura, S.; Iwata, T. Enzymatic Self-Biodegradation of Poly(l-lactic acid) Films by Embedded Heat-Treated and Immobilized Proteinase K. *Biomacromolecules* **2020**, *21* (8), 3301−3307.
(31) Khan, I.; Nagarjuna, R.; Dutta, J. R.; Ganesan, R. Enzyme-Embedded Degradation of Poly(ε-caprolactone) using Lipase-Derived from Probiotic Lactobacillus plantarum. *ACS Omega* **2019**, *4* (2), 2844−2852.
(32) Craik, C. S.; Page, M. J.; Madison, E. L. Proteases as therapeutics. *Biochem. J.* **2011**, *435* (1), 1−16.
(33) Zinger, A.; Koren, L.; Adir, O.; Poley, M.; Alyan, M.; Yaari, Z.; Noor, N.; Krinsky, N.; Simon, A.; Gibori, H.; Krayem, M.; Mumblat, Y.; Kasten, S.; Ofir, S.; Fridman, E.; Milman, N.; Lübtow, M. M.; Liba, L.; Shklover, J.; Shainsky-Roitman, J.; Binenbaum, Y.; Hershkovitz, D.; Gil, Z.; Dvir, T.; Luxenhofer, R.; Satchi-Fainaro, R.; Schroeder, A. Collagenase Nanoparticles Enhance the Penetration of Drugs into Pancreatic Tumors. *ACS Nano* **2019**, *13* (10), 11008−11021.
(34) Carson, C. C., 3rd; Sadeghi-Nejad, H.; Tursi, J. P.; Smith, T. M.; Kaufman, G. J.; Gilbert, K.; Honig, S. C. Analysis of the clinical safety of intralesional injection of collagenase Clostridium histolyticum (CCH) for adults with Peyronie's disease (PD). *BJU Int.* **2015**, *116* (5), 815−22.
(35) Rockwood, D. N.; Preda, R. C.; Yücel, T.; Wang, X.; Lovett, M. L.; Kaplan, D. L. Materials fabrication from Bombyx mori silk fibroin. *Nat. Protoc.* **2011**, *6* (10), 1612−1631.

https://doi.org/10.1021/acsbiomaterials.3c01758
ACS Biomater. Sci. Eng. 2024, 10, 2607−2615